

## High Energy Astrophysical Techniques

---

**Rosa Poggiani\***

*Università di Pisa and Istituto Nazionale di Fisica Nucleare, Sezione di Pisa*

*E-mail: [rosa.poggiani@unipi.it](mailto:rosa.poggiani@unipi.it)*

Multi-messenger astrophysics combines multifrequency astronomy in the electromagnetic domain with non photonic information carriers, gravitational waves, neutrinos, cosmic rays, to provide complementary information about cosmic sources. The present paper reviews the recent developments in the instrumentation and the first results of multi-messenger astronomy: the detection of a binary neutron star merger and of high energy neutrinos from a cosmic source.

*Late submission of the contribution at Frontier Research in Astrophysics - III (FRAPWS2018)*

*Frontier Research in Astrophysics - III (FRAPWS2018)*

*28 May - 2 June 2018*

*Mondello (Palermo), Italy*

---

\*Speaker.

## 1. Introduction

The astronomical observations have been performed, for a long time, using the variety of probes provided by the electromagnetic spectrum, extending from the radio wavelengths to the X-rays and gamma rays, in the context of multi-wavelength astronomy. The majority of astrophysical sources emit electromagnetic radiation, with the remarkable exception of black holes. Other information carriers belong to the world of particle physics: cosmic rays, neutrino, dark matter. The latest addition to the astrophysical probes is gravitational radiation. Each information carrier in multi-messenger astronomy probes different physical mechanisms contributing to the knowledge of astrophysical sources. The combination of the observations with different probes is completed by the ongoing surveys over the whole electromagnetic spectrum and the building of object catalogs, containing information about position, fluxes, spectra. Time domain astronomy investigates the variability of targets and the appearance of new sources. Cosmic rays are associated, if Galactic, with supernovae explosions, and with Active Galactic Nuclei if extra-galactic. High energy gamma rays and neutrinos are produced in the interactions of cosmic rays with the environment. Being neutral, these probes preserve the information on the direction of the original source.

A new age of multi-messenger astrophysics has started after the observation of the gravitational wave emission from the mergers of a binary black hole [5] and a binary neutron star system [11] and the detection of the first high-energy neutrino from a source [110]. Multi-messenger astronomy allows to investigate extreme environments and compact sources at all scales: black holes, neutron stars, binary black hole and neutron star mergers, active galactic nuclei etc. The combination of different probes is the key. In fact, the merger of compact objects produces gravitational waves and, if neutron stars are involved, electromagnetic emission; the stellar core collapse in supernovae produces electromagnetic emission and low energy neutrinos and, if not axisymmetrical, gravitational waves; energetic cosmic rays produce neutrinos in their interactions; accretion processes around compact objects produce electromagnetic radiation.

Multi-messenger astronomy relies on the detectability of the source emission with different instruments and on their coordination. The discovery of variability in a known high energy astrophysical source or the appearance of a new one requires observations over a common time interval, demanding for a rapid dissemination of the event for the follow-up to provide the characterization of the event type. The multi-messenger observations involve the synergy of large and small facilities, ranging from large telescopes and interferometers down to meter size telescopes [94].

The sensitivity of modern instruments is now allowing to investigate not only signals from astrophysical sources, but also backgrounds. Blazars can explain a large fraction of gamma ray background, but only a small part of neutrino background. Cosmic rays, gamma rays and neutrinos are closely tied, since the last two are produced in the interactions of the first ones.

The following sections will present the rainbow of the different astronomies that compose multi-messenger astronomy. The variety of information carriers and the broad energy ranges demand for different instruments and different observational techniques, that will be reviewed. High energy observatories routinely provide light curves of objects and sky maps. Some case studies will be presented: GW150914, GW170817, IceCube-170922A.

## 2. Astrophysical Messengers

The Spectral Energy Distribution (SED) describes the flux/flux density/luminosity of an astrophysical source as a function of energy/frequency/wavelength. The construction of a SED requires the combination of different instruments operating in the different regions of the spectrum and requires their intercalibration. The SED of Crab and of the blazar TXS 0506+056 are reported in Fig. 1 as examples.

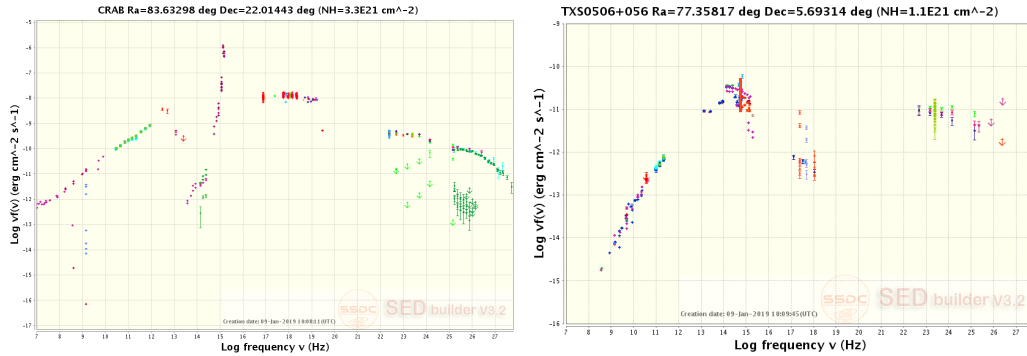


Figure 1: Spectral Energy Distribution of Crab (left) and TXS 0506+056; data from the SED Builder at <https://tools.ssd.casi.it/>

The various spectral regions provide information of different physical processes. The radio region provides the signature of non thermal processes. The optical region, the source of a large part of astrophysical information, probes thermal processes. The main physical mechanisms involved in high energy astrophysics are non thermal.

All electromagnetic observations face irreducible backgrounds. The measurements of the Extragalactic Background Light (EBL) over 20 decades in wavelength have been presented by [72], whose main results are summarized in Fig. 2. The Cosmic Microwave Background (CMB) has been measured with high precision. The Cosmic Optical Background is degraded by the presence of the zodiacal light produced by interplanetary dust. The Cosmic Infrared Background has a comparable intensity. The UV background is still partially unknown, due to the strong absorption of hydrogen, as shown by the gap in the SEDs in Fig. 1. The background at higher energies is the target of the present X-ray and gamma ray observatories and is believed to be mostly produced by unresolved active galactic nuclei.

The most energetic radiation cannot be detected if it is produced beyond specific horizons. High energy astrophysical photons interact with the Cosmic Microwave Background (CMB), the Extragalactic Background Light (EBL) (ultraviolet, optical, infrared) [78] and, for ground based detectors, also with the Earth atmosphere. The soft photon background produces a strong suppression of the radiation via the pair production process, that depends both on the photon energy and on the source redshift. The photon absorption in the energy range from 10 to  $10^{13}$  GeV is quite large, in particular around  $10^6$  GeV [78]. The horizon is shown in Fig. 3, left. High energy protons and nuclei interact via photo-pion production, pair creation and redshift losses [103]. A spectral steepening at about  $10^{19}$  eV, the GZK cut-off is expected [97], [188]. The attenuation length for protons is shown in Fig. 3, right.

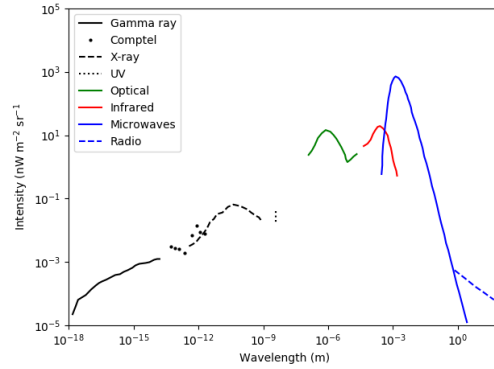


Figure 2: Intensity of the extragalactic background reported as  $\nu I_\nu$  ( $\text{nW m}^{-2} \text{sr}^{-1}$ ) as a function of the radiation wavelength in meters; data from [72]

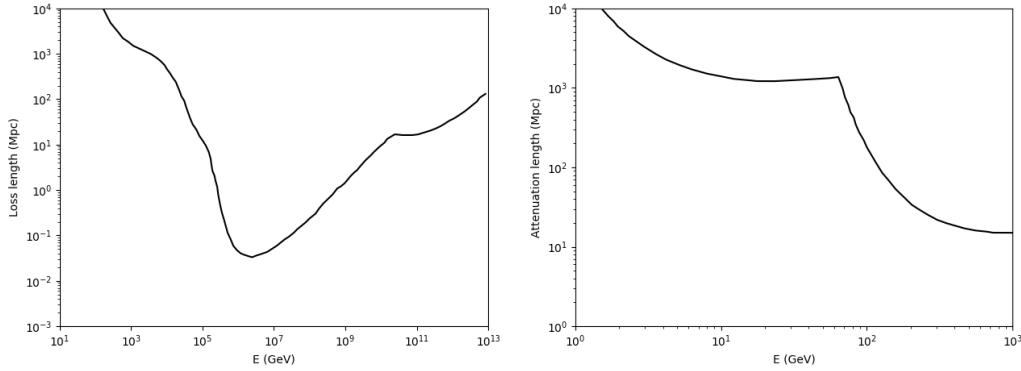


Figure 3: Left: distance in Mpc at which the optical depth corresponds to a photon survival probability of  $e^{-1}=0.37$  (data from [78]). Right: proton attenuation length vs. energy (data from [103])

The high energy electromagnetic radiation and cosmic rays can be detected with space based instruments (direct detection) or ground based instruments (indirect detection). In the latter case, they are detected through the products of their interactions with the atmosphere. High energy gamma rays produce, via pair production and bremsstrahlung, an electromagnetic shower containing high energy photons, electrons and positrons. High energy protons and nuclei produce, via hadronic interactions, charged and neutral pions, nuclear fragments and so on; charged pions decay into muons and neutrinos, while neutral pions decay into gamma rays, thus the hadron shower contains electromagnetic sub-showers. The ground based detection of the products of high energy gamma rays and cosmic rays uses the direct detection or on the Cherenkov radiation of charged particles or fluorescence radiation in the atmosphere.

### 3. Astrophysics with Cosmic Rays

Cosmic rays are charged particles with an astrophysical origin. The spectrum of cosmic rays, reported in Fig. 4, extends up to  $10^{20}$  eV, several orders of magnitude above the typical LHC energies. Cosmic rays incident on the Earth atmosphere include electron, protons and nuclei. Among

them, electrons, protons and some nuclei (He, C, O, Fe) are considered primary cosmic rays accelerated at the original sources, while other nuclei (Li, Be, B) not produced by nucleosynthesis are considered secondary cosmic rays. Positrons and antiprotons are also considered secondaries. The incoming cosmic rays are affected by the solar wind, that deviated the lower energy component, producing an anticorrelation with the solar activity. The less energetic cosmic rays are also more affected by the geomagnetic field.

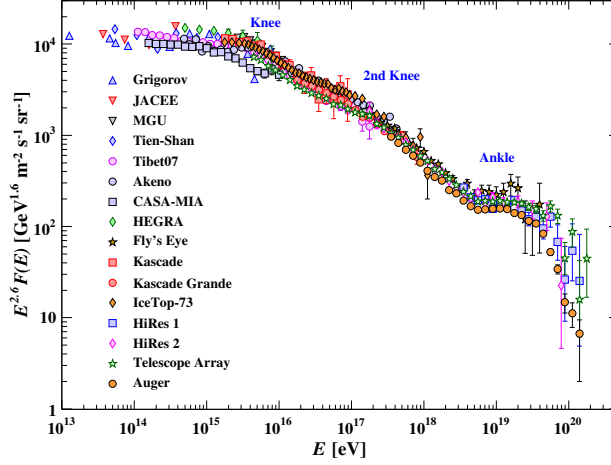


Figure 4: The all particle flux as a function of the energy per nucleon; adapted from [147]

With the exception of the low energy region where modulation by solar wind occurs, the energy spectrum of cosmic rays follows a power law with a spectral index of 2.7 up to the knee energy, about  $10^{16}$  eV, and a steeper index up to the ankle energy, about  $10^{18}$  eV [147]. Nearly 74% of the primary nucleons are protons, with about 70% of the rest are helium nuclei.

The acceleration of Galactic cosmic rays, with energies up to the knee energy, is believed to occur via the Fermi acceleration mechanism at the sites of supernova remnants. The propagation is governed by diffusion [176]. The more energetic cosmic rays are believed to have an extragalactic origin, with a probable association with active galactic nuclei.

The maximum energy  $E_{max}$  of an accelerated particle is defined by the Hillas criterion:

$$E_{max} = qBR \quad (3.1)$$

where  $q$  is the charge,  $B$  the magnetic field,  $R$  the size of the acceleration region; the Larmour radius must not exceed the size of the accelerator.

The Ultra High Energy Cosmic Rays are detected with ground based instruments that measure the products of their interaction with air molecules, the hadron shower. The rapid drop in the flux of the more energetic cosmic rays requires the realization of instruments covering large areas. The showers are reconstructed using three main techniques. The Air Shower Arrays measure the shower size  $N_e$ , the muon number  $N_\mu$  and the lateral distribution of the shower particles, using

an array of detectors deployed over large areas. The other two techniques rely on the radiation involved in the interaction of shower particles with the atmosphere. The Cherenkov instruments detect the Cherenkov radiation emitted by the high energy charged particles of the shower, while the fluorescence detectors measure the fluorescence of nitrogen molecules excited by the charged particles. The Cherenkov radiation is highly collimated, while fluorescence radiation is emitted isotropically, allowing the lateral observation of showers. A recent addition is the detection of radio-frequency emission of shower particle via geosynchrotron emission. The position of the shower maximum  $X_{max}$  depends on the mass of the primary nucleus, being larger for proton induced showers than for nuclei induced showers.

The Pierre Auger Observatory <sup>1</sup> (Fig. 5) is located in Argentina and consists of an array of 1660 water Cherenkov telescopes (Surface Detector, SD) and 27 air fluorescence telescopes (Fluorescence Detector, FD), deployed over 3000 km<sup>2</sup> to detect cosmic rays in the energy region above 10<sup>17</sup> eV [1]. The Surface Detector measures photons and charged particles at ground level, while the fluorescence detector monitors the longitudinal evolution of air shower. The observatory has been recently completed with the addition of the Auger Engineering Radio Array (AERA) for the detection of radio emission from air showers [105].

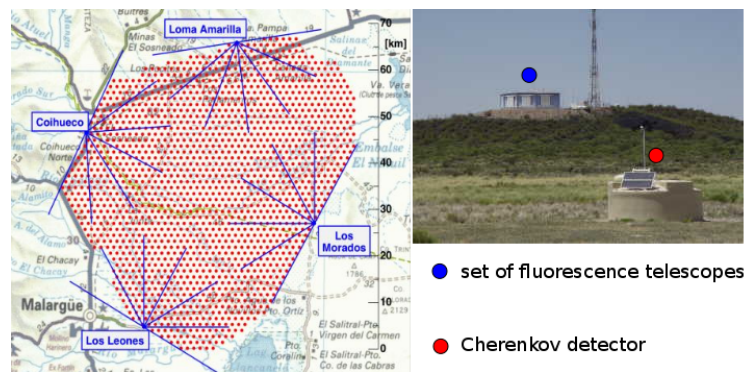


Figure 5: The Auger Observatory; Credits: <http://auger.org>)

The cosmic ray spectrum measured by the Auger Observatory [87] shows the ankle feature at  $5.08 \pm 0.06 \pm 0.8$  EeV and a flux suppression at higher energies. The chemical composition of cosmic rays is lighter in the range from 10<sup>17.2</sup> to 10<sup>18.3</sup> eV, as expected for a transition from a Galactic heavy composition to an extragalactic light composition. The average mass of primaries increases with energy [2], [96], [151]. The results are in agreement with the results of the TA experiment [119].

Space based detectors target the composition of the less energetic cosmic rays and search for antimatter in space. The common denominator of space based instruments is the combination of detectors that are routinely found at collider experiments: a calorimeter for energy reconstruction and a magnetic spectrometer for particle tracking and charge separation. The constraints of space experiments on size and mass of the payload force the reduction of the calorimeter thickness and of the magnet size. Transition Radiation Detectors (TRDs) are used to measure the Lorentz factor

<sup>1</sup><https://www.auger.org/>

of the particle, a proxy of its energy. The combination of the above measurements allows the separation of different species.

AMS-02 <sup>2</sup> (Fig. 6, left) is operating on the International Space Station (ISS). It hosts a large permanent magnet for the central Tracker that measures the curvature of charged particles with more than two thousands double sided microstrip detectors. A Time Of Flight (ToF) system based on scintillator paddles aligned along orthogonal directions measures the transit time of the particles and triggers the other detectors, allowing antimatter discrimination. The TRD provides the measurement of the  $\Gamma$  factor for protons and electrons of a given energy, improving the discrimination of positrons against protons. The Electromagnetic CALorimeter (ECAL), made of alternating lead and scintillating fiber layers (total thickness of 16 radiation lengths) provides a 3D reconstruction of the shower shape, allowing the separation of positron and proton induced showers and the reconstruction of the direction of the incoming particle with a precision of a few degrees.

The PAMELA <sup>3</sup> (Fig. 6, center) instrument contains a magnetic spectrometer with a NdFeB magnet equipped with planes of double sided microstrip silicon trackers to measure the trajectories of the incident particles, an electromagnetic sampling Si/W calorimeter and a scintillator for the shower tails. The ToF system consists of three groups of segmented scintillator planes.

DAMPE <sup>4</sup> (Fig. 6, right) consists of a plastic scintillator strip detector (PSD) as anti-coincidence detector, followed by a Si-W tracker-converter (STK), with six tracking double layers of single sided silicon strip detectors. Tungsten plates are mounted in front of tracking layers for photon conversion. The STK is followed by an imaging calorimeter with a thickness of about 31 radiation lengths, made of BGO bars arranged as an hodoscope. The thickness of the combined BGO calorimeter and STK tracker is about 33 radiation lengths, the largest for a space based calorimeter.

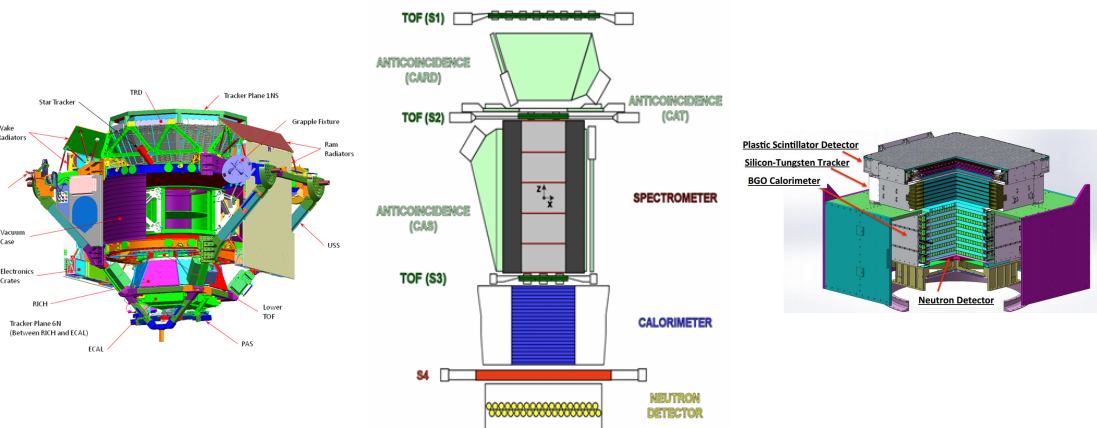


Figure 6: Direct cosmic ray detection in space: AMS-02 (credits: <https://ams.nasa.gov/>), PAMELA (credits: <https://pamela-web.web.roma2.infn.it/>), DAMPE (credits: <http://dpnc.unige.ch/dampe/>)

<sup>2</sup><https://ams.nasa.gov/>

<sup>3</sup><https://pamela-web.web.roma2.infn.it/>

<sup>4</sup><http://dpnc.unige.ch/dampe/>

#### 4. X-ray and gamma ray astronomy

The sensitivities of different X-ray and gamma ray instruments that will be described in the following is shown in Fig. 7.

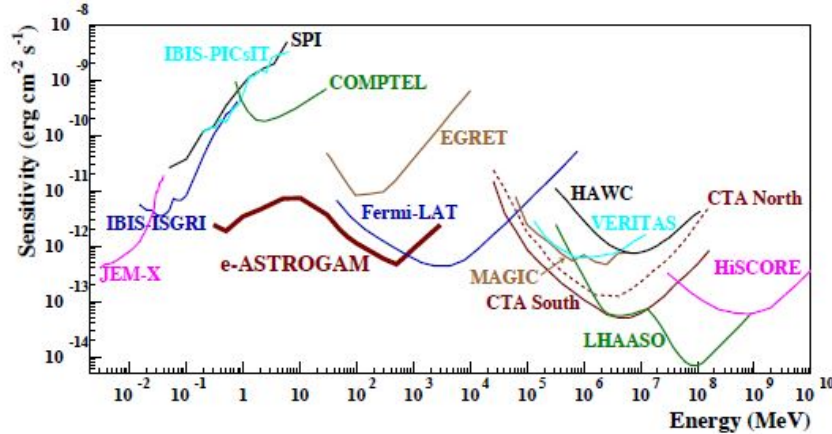


Figure 7: Point source continuum sensitivity of X-ray and gamma ray instruments (credits: <http://eastrogam.iaps.inaf.it/>)

The X-ray Universe includes thermal sources with temperatures of  $10^6$  to  $10^7$  K (white dwarfs, neutron stars, supernova remnants, stellar coronae, galaxy clusters) and non thermal sources (pulsars, supernovae, active galactic nuclei). The detection of X-rays from astrophysical sources requires operation in space, since the atmosphere is opaque to X-rays. Since X-rays cannot be focused with refractive elements, the soft X-rays are detected using grazing incidence telescopes (Fig. 8), an array of concentric paraboloid mirrors where X-ray photons undergo reflection with a very small angle with respect to the surface, followed by an array of hyperboloid mirrors that focus the radiation onto a focal plane. The solution has been adopted in the Chandra<sup>5</sup>, XMM-Newton<sup>6</sup>, eROSITA<sup>7</sup> (Fig. 8). The future instrument ATHENA<sup>8</sup> will use silicon pore optics for photon focusing.

The most common detectors in the focal plane of X-ray telescopes are CCDs, that detect individual X-ray photons, recording their arrival time, position and energy. CCDs for X-rays have intrinsic energy resolution capability for spectroscopy. Grating configurations similar to those found in optical spectrographs are used for achieving high resolution, as in Chandra and XMM-Newton. ATHENA will use X-ray Integral Field Units.

The telescopes for hard X-rays, about 100 keV, cannot rely on photon focusing and use coded aperture masks, where radiation enters the instrument through a mask with a pattern of opaque and transparent sections producing a shadow: sources are extracted with deconvolution techniques. The solution has been adopted in INTEGRAL<sup>9</sup> (Fig. 9, left) and Swift-BAT<sup>10</sup> (Fig. 9, right).

<sup>5</sup><http://chandra.harvard.edu>

<sup>6</sup><http://sci.esa.int/xmm-newton/>

<sup>7</sup><http://www.russianspaceweb.com/spektr-rg-erosita.html>

<sup>8</sup><https://www.the-athena-x-ray-observatory.eu/>

<sup>9</sup><https://www.cosmos.esa.int/web/integral>

<sup>10</sup><https://swift.gsfc.nasa.gov/>

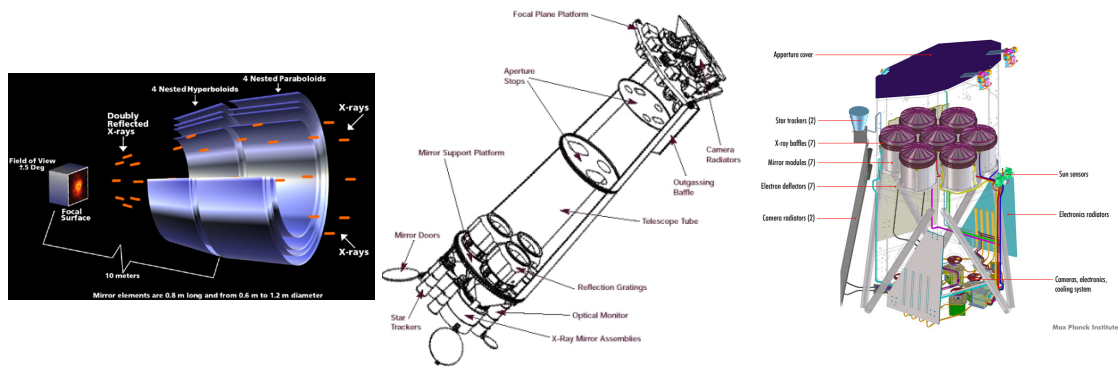


Figure 8: Grazing incidence telescopes: Chandra (credits: <http://chandra.harvard.edu/>); XMM-Newton (credits: <http://sci.esa.int/xmm-newton/>); eROSITA (credits: <http://www.russianspaceweb.com/spektr-rg-erosita.html>)

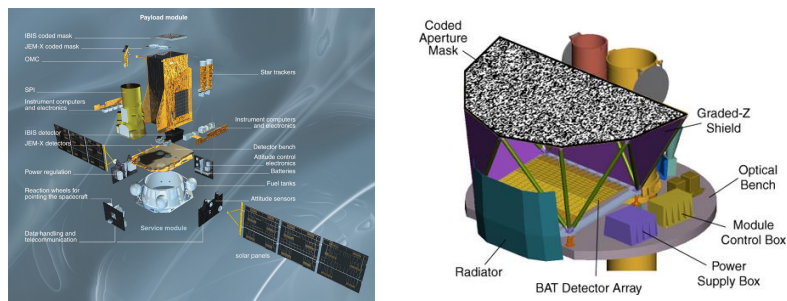


Figure 9: Coded mask telescopes: INTEGRAL (credits: <https://www.cosmos.esa.int/web/integral>) and Swift-BAT (credits: <https://swift.gsfc.nasa.gov/>)

X-ray observatories routinely provide all sky maps and long term light curves of objects. As an example, the map produced by Swift-BAT in the 105 months sky survey is show in Fig. 10.

X-ray polarimetry can provide information about strong gravity sources [55]. Polarimetric instruments are based on Compton scattering, Bragg scattering or photoelectric effect, covering the hard and soft X-ray regions [55]. Future missions include IXPE<sup>11</sup>, eXTP<sup>12</sup>.

The energy region from 1 MeV to about 30 MeV is still relatively unexplored, despite its relevance for nuclear processes, the physics of Gamma Ray Bursts and the signature of the 511 keV line from positron annihilation. The MeV region is investigated using Compton telescopes, that rely on the Compton scattering to estimate the energy and the direction of the incoming photon. A Compton telescope consists of two detector arrays. The top one is made with a low Z material, while the bottom one is made with an high Z material. Gamma rays undergo scattering in the top detector and are absorbed in the bottom one. The energy transferred to the electron in the Compton interaction is measured by the first detector, often a plastic scintillator. The energy of the scattered photon is measured in the bottom detector, a scintillating crystal or a semiconductor. The measured energies allow to estimate the Compton scattering angle. The COMPTEL telescope on

<sup>11</sup><https://ixpe.msfc.nasa.gov/>

<sup>12</sup><https://www.isdc.unige.ch/extp/>

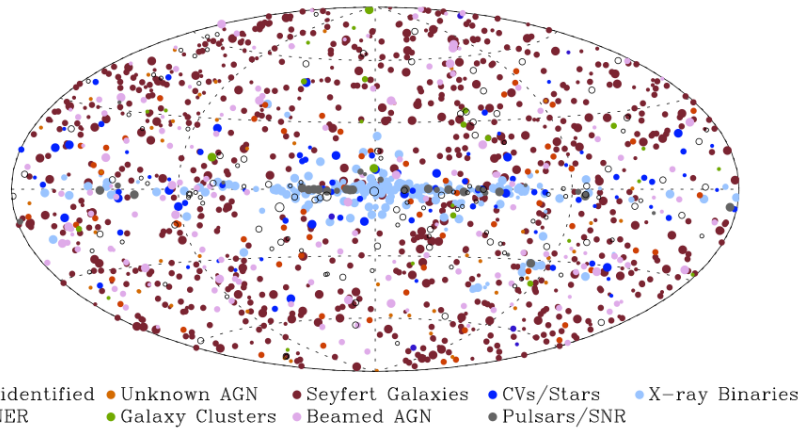


Figure 10: Swift-BAT 105 months all-sky survey (credits: <https://swift.gsfc.nasa.gov/results/bs105mon/>)

board of the Compton Gamma Ray Observatory is shown in Fig. 11. The energy interval from the region covered by COMPTEL to the low energy side is the target of the proposed e-ASTROGAM Observatory <sup>13</sup>.

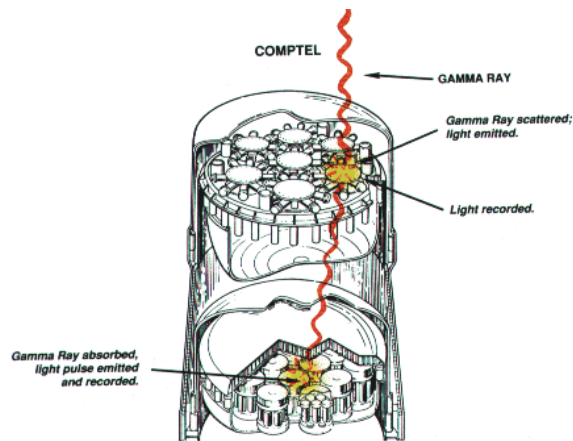


Figure 11: Schematics of the Compton telescope COMPTEL (credits: <https://www.sron.nl/missions-astrophysics/past/cgro-comptel>)

Gamma ray astrophysics is particularly suitable to probe the mechanisms of particle acceleration. Astrophysical gamma rays span a broad energy range. Due to the different instrumental techniques needed, the range is split into different energy bands: Low Energy (LE, 0.1-100 MeV), High Energy (HE, the GeV region) and Very High (VHE, TeV and above). For energies above some MeV, pair production becomes the dominant mechanism for photon detection, leading to the pair conversion telescopes. The direction and the energy of the incident gamma ray are reconstructed by combining the tracking of the direction of motion of the pair and the energy measurement with

<sup>13</sup><http://eastrogam.iaps.inaf.it/>

a calorimeter. The Fermi-LAT <sup>14</sup> (Fig. 12, left) uses a tracker made of layers of an absorbing material with high atomic number and silicon strips arranged along two orthogonal directions that reconstruct the x,y coordinates of the electron/positron in each layer. The energy of the particles is measured by a cesium iodide calorimeter. The Fermi-GBM <sup>15</sup> (Fig. 12, right) includes twelve sodium iodide (NaI) scintillators and two bismuth germanate (BGO) scintillators, sensitive in the regions from a few keV to 1 MeV and from 150 keV to 30 MeV, respectively. The NaI detectors provide burst triggers and localization, while the BGO detectors have a sensitivity overlapping those of NaI at low energies and of the Fermi-LAT at high energies.

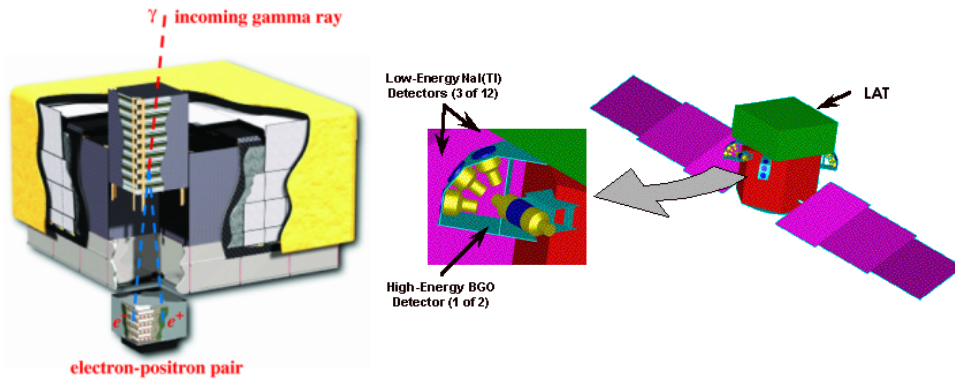


Figure 12: Fermi-LAT (left, credits: <https://glast.sites.stanford.edu/>); Fermi-GBM (right, credits: <https://fermi.gsfc.nasa.gov/science/instruments/gbm.html>)

An example of gamma ray astronomy, Fermi-LAT has measured the diffuse gamma ray background in the region between 100 MeV and 820 GeV [25], whose extragalactic counterpart can be explained by blazars [27] (Fig. 13).

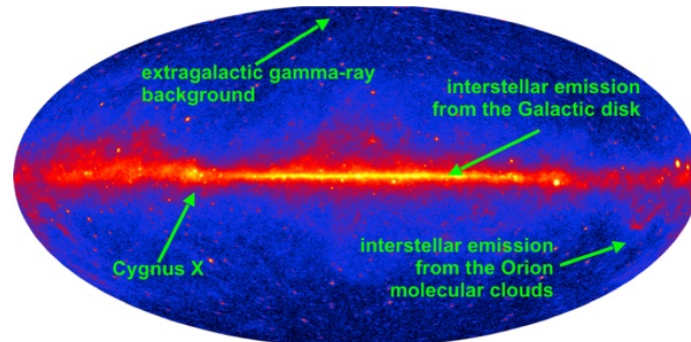


Figure 13: Diffuse gamma ray emission observed by Fermi-LAT (credits: <https://fermi.gsfc.nasa.gov/science/eteu/diffuse/>)

The low rates of gamma ray fluxes above one hundred GeV preclude the use of space based instruments, whose effective areas are relatively small. The most energetic gamma rays are detected observing the electromagnetic cascades produced in the interaction with the atmosphere. The direction of the incident gamma ray is estimated from the direction of the shower, while the energy of

<sup>14</sup><https://glast.sites.stanford.edu/>

<sup>15</sup><https://fermi.gsfc.nasa.gov/science/instruments/gbm.html>

the gamma ray is proportional to the number of particles in the shower. The shower properties are measured with two different techniques. The first approach is the detection of the Cherenkov emission produced by the electrons and positrons in the shower. The Imaging Atmospheric Cherenkov Telescopes (IACT) are reflectors equipped with photon detectors at their foci. The Cherenkov signal is highly collimated, with angles of the order of one degree, and very short, with a duration of the order of a few ns. The short duration and the high collimation of the Cherenkov flash are used to discriminate the signal from the sky background. The intensity of the Cherenkov radiation is proportional to the number of particles and is a proxy of the energy of the progenitor gamma ray. HESS<sup>16</sup> and MAGIC<sup>17</sup> are examples of Cherenkov telescope arrays operating in the energy band from 30 GeV to 10 TeV, with reflector diameters up to 30 meters. The future CTA observatory<sup>18</sup> will cover an energy range from 20 GeV to 300 TeV, with 40 medium size telescopes (100 GeV-10 TeV) over two sites, 8 large telescopes (below 100 GeV) and 70 small telescopes (above 10 TeV). The observatory will be split, with 19 instruments in the Northern hemisphere and 99 in the Southern one. The main background in ground based gamma ray detectors is given by the showers produced by cosmic rays, that include electromagnetic subshowers. The hadron showers from protons and nuclei contain pions and heavy particles, in addition to electron and positrons. The electromagnetic and hadron showers are discriminate on the basis of their morphology, since hadron showers have a larger angular spread compared to the electromagnetic showers.



Figure 14: MAGIC (left, credits: <https://magic.mpp.mpg.de/>); CTA (right, credits: <https://www.eso.org/public/teles-instr/paranal-observatory/cta/>)

The second approach is the use of detectors distributed over large areas, to probe the number of particles reaching ground, proportional to the energy of the incident gamma ray. The most common detector is the water Cherenkov, where particles with a speed larger than the Cherenkov threshold produce Cherenkov radiation. An example is the HAWC experiment<sup>19</sup>.

The TeV sky presently contains more than two hundred sources (Fig. 15).

## 5. Neutrino Astrophysics

The spectrum of neutrinos encompasses a broad range of energies, as shown in Fig. 16.

Astrophysical neutrinos from the Sun or supernovae are in the MeV energy range and are produced in nuclear reactions. The detection of neutrinos from the Sun by the Homestake experiment

<sup>16</sup><https://www.mpi-hd.mpg.de/hfm/HESS/>

<sup>17</sup><https://magic.mpp.mpg.de/>

<sup>18</sup><https://www.cta-observatory.org>

<sup>19</sup><https://www.hawc-observatory.org/>

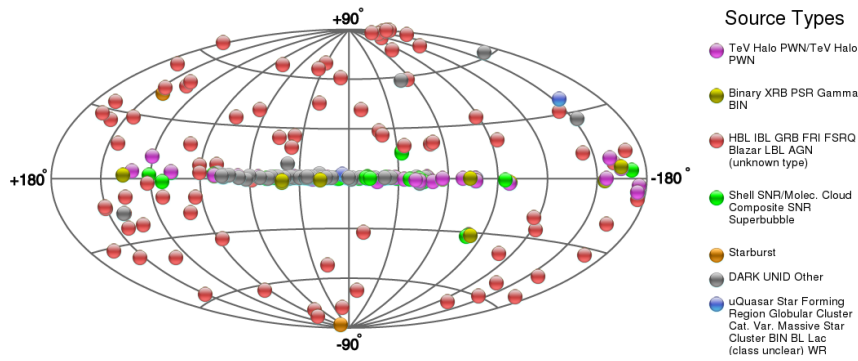
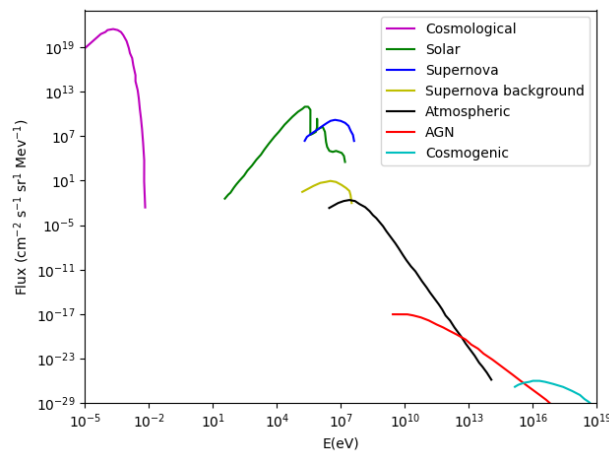
Figure 15: The TeV sky (credits: <http://tevcat.uchicago.edu/>)

Figure 16: The neutrino energy spectrum (data from [175])

triggered the solar neutrino problem [77]. Neutrinos from the supernova SN 1987A were observed by the Kamiokande II [104], IMB [100] and Baksan [45] experiments.

High energy neutrinos with energies in the GeV range or above are produced in the interactions of protons or ions with matter. Energetic neutrinos are a suitable probe to reconstruct the sources of cosmic rays, since they are not deflected by magnetic field. Reviews of high energy neutrino astrophysics have been presented by [118], [102], [40]. The detection of energetic neutrinos requires large volume detectors, typically water or ice, for measuring the Cherenkov radiation of the charged particles (usually muons) produced in the neutrino interactions. The main background is given by the showers produced by cosmic rays and is reduced by requiring that the interaction occurs inside the detector or from the Earth direction. In addition, the sensitive part of the large volume detector is at a great depth in ice or in water. Cosmic ray showers contain neutrinos, the atmospheric neutrinos, that are not shielded by the Earth and can be rejected by looking at coincidence with muons. Currently operating and future instruments include ANTARES [36], Baikal [57], KM3Net [30], the South Pole based detector IceCube [102], [24]. ANTARES<sup>20</sup> and KM3Net

<sup>20</sup><http://antares.in2p3.fr/>

<sup>21</sup> rely on the Cherenkov effect of charged particles produced in neutrino interactions in deep water. The IceCube detector (Fig. 17) <sup>22</sup> consists of about one cubic kilometer of ice at depths ranging from 1.4 to 2.4 km at the South Pole, equipped with 5160 optical photomultipliers arranged along 86 strings [24]. IceCube is able to detect all neutrino flavors, that exhibit different signatures. Muon neutrinos interacting via the charged current reaction produce a Cherenkov track, while the other flavors produce showers. The arrival direction can be reconstructed at the level of one degree for tracks and about ten degrees or more for showers.

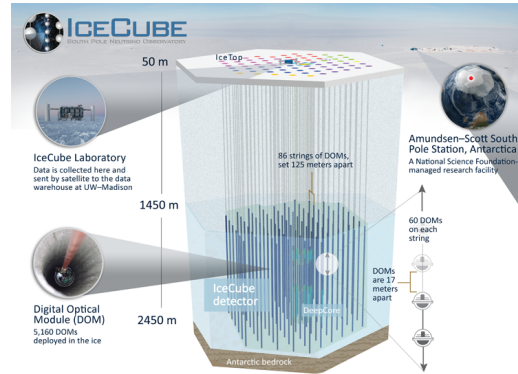


Figure 17: The IceCube detector (credits: <https://icecube.wisc.edu/>)

IceCube has observed a diffuse flux of neutrinos in the energy interval from 100 TeV to 1 PeV [3], [108], whose spectrum can be described by a broken power law with a break at around 200 TeV. The all sky map built using 10 years of data [4] is shown in Fig. 18.

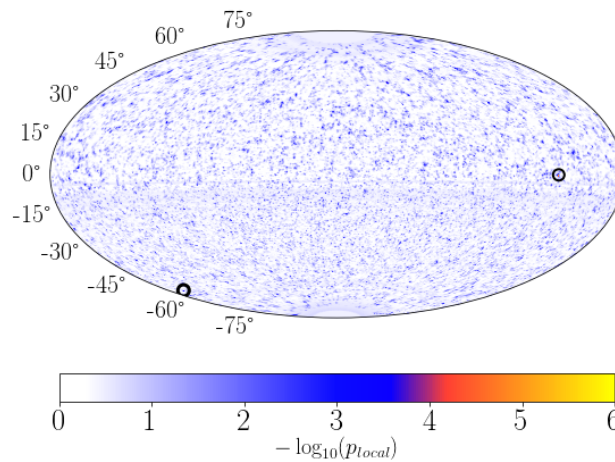


Figure 18: The IceCube sky (credits: <https://icecube.wisc.edu/>)

The detection of neutrinos from the blazar TXS 0506+056 is discussed in detail in Section 10.3.

<sup>21</sup><https://www.km3net.org/>

<sup>22</sup><https://icecube.wisc.edu/>

## 6. Gravitational Astrophysics

The gravitational wave spectrum extends over a broad frequency band (Fig. 19), that so far has been explored only in the high frequency region by the Advanced LIGO<sup>23</sup> and Advanced Virgo<sup>24</sup> interferometers, a network of three ground based detectors operating in the frequency range from a few Hz to some kHz.

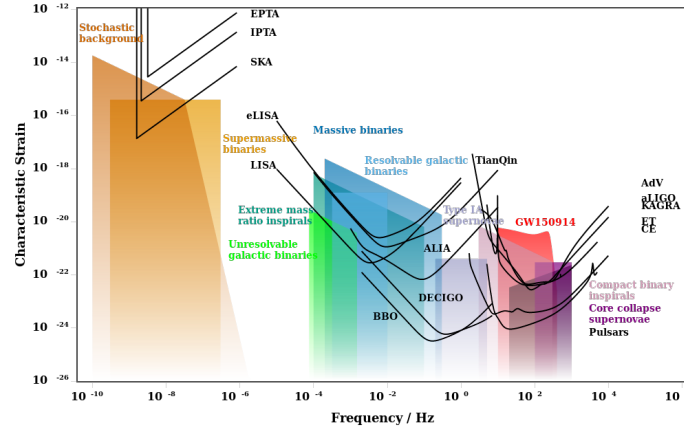


Figure 19: The gravitational wave spectrum (credits: <http://gwplotter.com/>)

The discovery of gravitational waves from the binary black hole merger GW150914 announced by LIGO in 2016 [5] was followed by the detection of the similar events GW151226 [7], [8], [9], [10] and GW170729, GW170809, GW170818 and GW170823 [21]. An extensive search with three different algorithms for coalescing compact binaries with component masses above one solar mass in the O1 and O2 observing runs of the advanced gravitational wave detector network has produced the first Gravitational Wave Transient Catalog, GWTC-1 [21]. During the first run (O1) three binary black hole mergers were detected. During the second observing run (O2) a binary neutron star merger and seven binary black hole mergers were detected [21]. The detected binary black holes have total masses between  $18.6^{+3.1}_{-0.7} M_{\odot}$  and  $85.1^{+15.6}_{-10.9} M_{\odot}$  (Fig. 20, left) with distances ranging from  $320^{+120}_{-110}$  Mpc to  $2750^{+1350}_{-1320}$  Mpc [21]. The estimated merger rates are  $110\text{-}3840 \text{ Gpc}^{-3} \text{ y}^{-1}$  for binary neutron stars,  $9.7\text{-}101 \text{ Gpc}^{-3} \text{ y}^{-1}$  for binary black holes and below  $610 \text{ Gpc}^{-3} \text{ y}^{-1}$  for neutron star-black hole systems [21]. The majority of the detected black holes have low spins or misaligned spins with respect to the orbital momentum (Fig. 20, right), while black holes in X-ray binaries can have very large spins.

The first binary neutron star merger, GW170817, occurred on 2017 August 17 [11] and was followed by the short Gamma Ray Burst GRB 170817A after 1.7 seconds. The gravitational detection triggered a multi-messenger campaign over the electromagnetic spectrum and with neutrinos. The multi-messenger observations of GW170817 and the impact on fundamental physics and astrophysics are discussed in Section 10.2.

The third LIGO-Virgo observing run (O3) started on April 1, 2019 and several candidate mergers have been detected. The LIGO-Virgo alerts and event maps in O3 are public. The gravitational

<sup>23</sup><https://www.ligo.org/>

<sup>24</sup><http://www.virgo-gw.eu/>

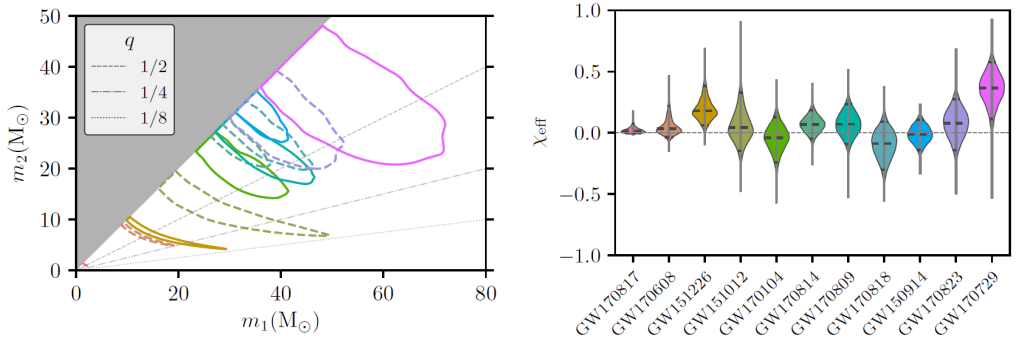


Figure 20: Masses (left) and spins (right) of the binary mergers detected by LIGO/Virgo during O1, O2 observing runs (adapted from [21])

event candidates are stored in the Gravitational Wave Candidate Event Database GraceDb<sup>25</sup> and distributed by the Gamma-Ray Coordinate Network GCN<sup>26</sup>. The number of gravitational wave observatories is steadily increasing. The Japanese KAGRA interferometer<sup>27</sup> has completed construction and is expected to join LIGO and Virgo during the O3 run. India has planned LIGO India for the beginning of next decade.

The third generation ground based interferometers are expected to be operative after 2030, improving the sensitivity by one order of magnitude, relying to cryogenics (test masses and part of suspensions) to reduce the thermal noise. The Einstein Telescope<sup>28</sup> will have 10 km arms, will be operated underground to reduce seismic noise and with cryogenic suspensions [158]. The cryogenic LIGO Voyager will operate in the same LIGO infrastructure [169]. The Cosmic Explorer (CE) will have 40 km arms and one cryogenic silicon detector [15]<sup>29</sup>.

The very low frequency region will be explored by the space based interferometers LISA [46]<sup>30</sup> and TianQin [112], that will be sensitive to resolved binaries, massive binary black hole mergers, but also to the final stages of the merger of stellar black holes, that could trigger the operation of ground based interferometers in multifrequency gravitational wave astronomy [168].

## 7. Dark Matter

The evidence for Dark Matter was initially suggested by astrophysical observations of the galactic rotation curves, where the rotation velocity becomes approximately constant instead of decreasing with radius [163] and suggests the presence of a dark halo. The estimated local Dark Matter density in the Earth neighborhood is of the order of  $0.4 \text{ GeV cm}^{-3}$  [147]. There are several candidates for Dark Matter, that must have weak interactions with electromagnetic radiation,

<sup>25</sup><https://gracedb.ligo.org>

<sup>26</sup><https://gcn.gsfc.nasa.gov/>

<sup>27</sup><https://gwcenter.icrr.u-tokyo.ac.jp/en/>

<sup>28</sup><http://www.et-gw.eu/>

<sup>29</sup><https://cosmicexplorer.org/>

<sup>30</sup><https://www.elisascience.org/>

among them axions, sterile neutrinos, primordial black holes and Weakly Interacting Massive Particles (WIMPs).

The axion particles have been proposed to solve the strong CP problem in QCD [148], [149]. They can be detected through the axion to photon conversion process. The ADMX experiment has excluded the range of axion-photon couplings in the mass range from 2.66 to 2.81  $\mu\text{eV}$  [83]. Sterile neutrinos are expected to have keV masses [124] and could be detected through the mixing with standard neutrinos, that leads to a radiative decay with monochromatic photons with an energy that is one half of the neutrino mass. There is an astrophysical evidence for a 3.5 keV line in the X-ray stacked spectra of galaxy clusters secured with XMM-Newton [65], that has not been confirmed by other X-ray observatories [39], [182]. Primordial black holes, formed before Big Bang Nucleosynthesis, are strongly constrained as Dark Matter candidates [66]. Baryonic matter could exist as MAssive Compact Halo Objects (MACHOs) [143], whose presence can be detected through the microlensing, but strong limits have been set, see e. g. the results of the MACHO survey [43]. It has been suggested that primordial black holes could give a relevant contribution to dark matter [67] and that the GW150914 event could be pointing to this class of dark matter [61]. Stellar mass black holes alone are not able to reproduce all dark matter [62], [89], [122]. If the gravitational wave event GW150914 was produced by the merger of primordial black holes, the expected merger rate exceeds the rate estimated by gravitational observations, unless primordial black holes are a small fraction of dark matter [164].

The WIMPs are particles with a mass in the range 10 GeV to some TeV, with the lightest supersymmetric particle (LSP), the neutralino [113] the strongest candidate so far. The WIMPs are expected to be gravitationally trapped inside galaxies with a Maxwellian velocity distribution, whose average value at the Sun position is of the order of a few hundreds kilometers per second. The main physical process used for the direct detection of WIMPs is the elastic scattering on nuclei. Since predictions for the WIMP masses range from 10 GeV to 10 TeV, the nuclei will have a recoil energy from 1 to 100 keV, demanding for low threshold detectors. The recoil spectrum is exponential, with a larger mean for more massive WIMPs. The cross section for on relativistic WIMPs is spin independent or spin dependent, scaling as the square of the nucleus mass and on the nuclear spin factor, respectively, thus high mass nuclei such as Xenon are the chosen materials for detectors. Since the expected rates are below 1 event  $\text{day}^{-1} \text{kg}^{-1}$ , detectors must be massive. The background is reduced using radio pure materials and placing detectors underground. WIMPs are expected show a daily forward/backward recoil asymmetry and an annual modulation of the detected recoils.

Different detector strategies have been adopted. Semiconductor detectors have been used in the CoGent experiment <sup>31</sup> (440 g Ge). The DAMA/LIBRA Collaboration <sup>32</sup>, using radio pure NaI scintillators, has claimed a signal in a 13 year observation, with the predicted annual modulation [60]. Liquid noble gas detectors usually rely on the detection of two physical effects, the scintillation and the ionization in the liquid to separate of nuclear and electron recoils. The family of XENON detectors at Gran Sasso has evolved from 10kg, 100 kg to one ton, in XENON1t <sup>33</sup>,

<sup>31</sup><https://cogent.pnnl.gov/>

<sup>32</sup><http://people.roma2.infn.it/dama/web/home.html>

<sup>33</sup><https://www.science.purdue.edu/xenon1t>

which set the best constraints on the interaction cross section [47]. Other detector operating with liquid Xenon are LUX<sup>34</sup> (370 kg) and PandaX<sup>35</sup> (500 kg). The DarkSide<sup>36</sup> detector relies on the principle of a two phase liquid argon Time Projection Chamber, that detects the scintillation and the ionization produced by recoiling nuclei. Other detectors operate at milliKelvin temperatures using the simultaneous measurement of ionization and phonons, to provide discrimination between nuclear and electron recoils, like SuperCDMS<sup>37</sup> and EDELWEISS<sup>38</sup>. On the other hand, the cryogenic detector CRESST<sup>39</sup> relies on scintillation to discriminate against background.

Since the interaction rate depends on the interaction cross section and on the WIMP mass, the limits on dark matter are usually presented as contours in the cross section vs. WIMP mass plot. The experimental status of the art, according to [166], is shown in Fig. 21,

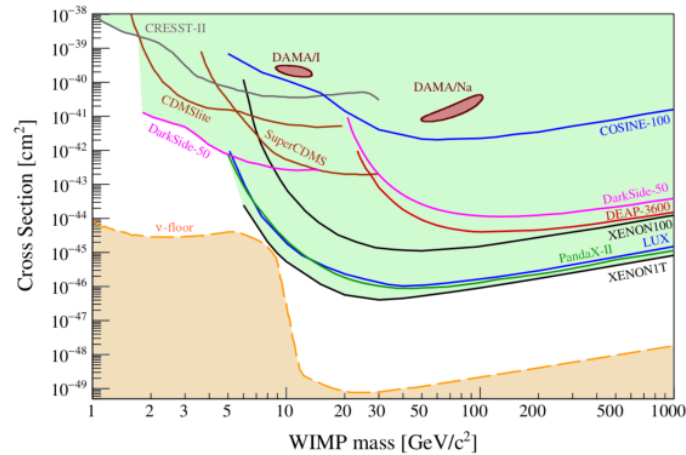


Figure 21: The parameter space for spin independent WIMP-nucleon cross section, where the dashed line is the irreducible neutrino floor from coherent neutrino-nucleus scattering (adapted from [166])

In addition to direct WIMP searches, there are several approaches for indirect searches. WIMPs can annihilate producing Standard Model particles, such as gamma rays, antiprotons, positrons, neutrinos. WIMPs could be decelerated and trapped in the Earth or the Sun, increasing the probability of annihilation and producing muon neutrinos, potentially detectable by SuperKamiokande and IceCube. Other indirect searches for dark matter are searching for gamma rays produced in astrophysical sources: the halo, the Galactic center, dwarf galaxies. The search for gamma rays excess is made difficult by the presence of astrophysical backgrounds. The region around the Galactic center hosts several gamma ray sources [28], among them the TeV source HESS J1745-290 [38]. An excess of GeV gamma rays around the Galactic center have been explained with WIMP annihilation [106]. The Fermi-LAT observations have constrained the annihilation of WIMPs in dwarf galaxies [26].

<sup>34</sup><http://luxdarkmatter.org/>

<sup>35</sup><https://pandax.sjtu.edu.cn/>

<sup>36</sup><http://darkside.lngs.infn.it/>

<sup>37</sup><https://supercdms.slac.stanford.edu/>

<sup>38</sup><http://edelweiss.in2p3.fr/>

<sup>39</sup><https://www.cresst.de/>

While the elemental composition of cosmic rays is dominated by protons and nuclei, there is also a fraction of antiparticles, positrons and antiprotons, that could be related to the annihilation of dark matter particles. The antiproton to proton ratio  $\bar{p}/p$  and the positron ratio  $e^+/(e^+ + e^-)$  are reported in Fig. 22 (left and right). The data of PAMELA [32] and AMS02 [33], [34] show a rise of the positron fraction above 10 GeV. The observations [31], [35] are consistent with the standard models for production and propagation of cosmic rays.

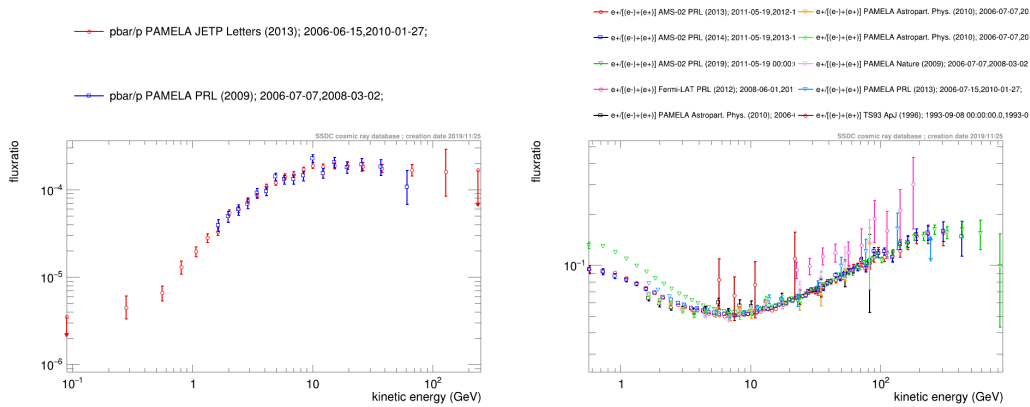


Figure 22: The antiproton to proton and the positron ratios; data from <https://tools.ssdc.asi.it/CosmicRays/>

## 8. Optical and Radio Astronomy

Optical astronomy plays a relevant role in high energy astrophysics: the detections of new transients are cross-checked against existing catalogs and archives for an accurate sky localization and to search for possible progenitors. Present optical astronomy involves large telescopes with apertures as large as ten meters, such as the Very Large Telescope (VLT)<sup>40</sup>. Sky surveys, differently from targeted astronomical observations of one or a few objects, provide systematic information about a large number of sources or some class of objects, that could become the subject of dedicated observations. Surveys provide catalogs of the sky and discover unexpected transients, and are in any case necessary to begin any other investigation. Spectroscopic surveys investigate the physical properties of sources detected in imaging surveys, providing their characterization, with abundances, radial velocities or redshift for extragalactic sources. The Sloan Digital Sky Survey<sup>41</sup> (SDSS) has produced multiband imaging of one third of the sky and secured spectra for more than three million astronomical objects. The astrometry mission Gaia<sup>42</sup> is producing the most accurate three dimensional map of the Milky Way [90]. The Data Release DR2 has provided the position, proper motion, multi-band photometry, radial velocities and parallaxes for nearly 1.7 billion stars [63].

New instruments are about to enter operation. The Large Synoptic Space Telescope<sup>43</sup> (LSST)

<sup>40</sup><https://www.eso.org/public/teles-instr/paranal-observatory/vlt/>

<sup>41</sup><https://www.sdss.org/>

<sup>42</sup><http://sci.esa.int/gaia/>

<sup>43</sup><https://www.lsst.org/>

will survey the Southern sky every few days. The LSST telescope is a three-mirror telescope with an aperture of 8.4m, equipped with active optics, with a wide field of view and fast slewing. The LSST camera is the largest digital camera ever built, with a size of 1.65m by 3m, sensitive from the near ultraviolet to near infrared, with a 3.5 degrees field of view. The space based EUCLID Observatory <sup>44</sup> will observe sky patches of about 400 square degrees every month, surveying each hemisphere every six months.

Planned instruments will have apertures in the range 30 to 40 meters. The European Extremely Large Telescope <sup>45</sup> (E-ELT) is a future 40 m class instrument that will become the largest optical/IR telescope in history [92]. The instrument will be a fully steerable five mirror system, providing diffraction limited operation. The Thirty Meter Telescope <sup>46</sup> will be a folded Ritchey-Chretien systems. Since the angular resolution of ground based telescope is limited by atmospheric seeing, adaptive optics will be an integral part of the instruments to achieve diffraction limited operation.

The James Webb Space Telescope (JWST) is a space based telescope [91] scheduled for launch in 2021. The telescope has an aperture of 6.5 m and hosts several instruments: the Mid-Infrared Instrument (MIRI), the Near-Infrared Spectrograph (NIRSpec), the Near-Infrared Camera (NIRCam), the Fine Guidance Sensor/ Near InfraRed Imager and the Slitless Spectrograph (FGS-NIRISS).

Smaller telescopes will still play a role, since they are able to provide long term monitoring of sources and prompt response to new transients [93]. The detection of transients relevant for high energy or gravitational astrophysics is performed by time domain facilities that rely on telescopes or network of telescopes with relatively small apertures. The Zwicky Transient Facility <sup>47</sup> (ZTF) [56] started operation in 2017 after the successful operation of the Palomar Transient Factory (PTF). The ZTF uses a camera with a field of view of 47 square degrees installed at the Samuel Oschin 48 inch Schmidt telescope and has the ability of scanning more than 3750 square degrees in an hour at the level of 20.5 mag. The ASAS-SN facility <sup>48</sup> [157] presently consists of a network of 24 telescopes with apertures of the order of 14 cm, distributed around the world, providing the survey of the whole visible sky every night. The MASTER network <sup>49</sup> aims to produce a fast sky survey with the observation of the whole sky over a single night down to a limiting magnitude of 19-20 [128].

Present radio astronomy is strongly focused on interferometry, combining several individual systems to improve the angular resolution, from the diffraction limit  $\sim \lambda/D$ , where  $D$  is the aperture diameter, to  $\sim \lambda/B$ , where  $B$  is the distance between the interferometer elements. The Very Large Array <sup>50</sup> (VLA) has a Y-like configuration, with nine 35 m parabolic dishes on each arm whose separation ranges from 1 to 36 km. The array provides observations from about 1 m to a few mm. The ALMA <sup>51</sup> observatory in Chile includes fifty four 12 meter diameter antennas whose distance

---

<sup>44</sup><http://sci.esa.int/euclid/>

<sup>45</sup><https://www.eso.org/public/teles-instr/elt/>

<sup>46</sup><https://www.tmt.org/>

<sup>47</sup><https://www.ztf.caltech.edu/>

<sup>48</sup><http://www.astronomy.ohio-state.edu/~assassin/index.shtml>

<sup>49</sup><http://observ.pereplet.ru/>

<sup>50</sup><https://science.nrao.edu/facilities/vla>

<sup>51</sup><https://www.almaobservatory.org/en/home/>

can be varied from 0.15 to 16 km and four additional 12 m and twelve 7 meter antennas. The array allows observations from about 10 mm to some cm. In the Very Long Baseline Interferometry (VLBI) technique, the single antennas are distributed over the whole Earth, achieving baselines up to  $10^4$  km. Using this technique, the Event Horizon Telescope <sup>52</sup> (EHT) Collaboration has produced the first image of the shadow of a black hole, the supermassive black hole at the core of M87 [86]. The forthcoming Square Kilometer Array <sup>53</sup> (SKA) will include some hundreds stations with baselines up to hundreds kilometers.

## 9. Time domain astrophysics

Time variability in sources involves time scales spanning several orders of magnitude, from milliseconds to centuries [81], [98]. Several systems show variability at subsecond scales: accreting systems containing a compact object, pulsars emitting optical radiation, oscillating neutron stars or white dwarfs [81]. Eclipsing binaries, Cepheids and RR Lyrae variables have periods smaller or of the order of days. Dwarfs novae show periodic outbursts with periods from months to years. Blazars and quasars show flares at intervals of years or decades, as the outbursts of recurrent novae [98]. The efforts of time domain astrophysics are focused on achieving high temporal cadence over the whole electromagnetic spectrum and to digitize the plate archives back to one century ago, to investigate both superfast processes and processes varying over decades [98], [107]. The science drivers for time domain astronomy, that include the measure of fundamental cosmological constants, the frequency of compact binary mergers, the physics of supernovae, have been discussed by [187].

An example of interest for high energy astrophysics is the gamma ray flare of PKS 2155-304 in July 2006 [37], with the observation of a variability up to 600 seconds and distinct bursts on timescales of about 200 seconds. Optical microvariability at minutes scales has been observed in blazars by different authors (see e.g. [134], [159], [185]). The time scale of optical microvariability can constrain the size of the emission region [186] and the Doppler factor of blazars. The time scales of microvariability in the optical and gamma ray domains allows to discriminate whether they have a common origin or not.

Different instruments in operation are performing high time cadence optical observations at medium and large telescopes. UltraCam and UltraSpec use CCDs [79] achieving a time resolution of a few milliseconds. The Single photon Avalanche Photo-Diodes (SPADs), that allow to achieve a time resolution in the nanosecond region, are used in the OPTIMA [114] and Iqueye [51] photometers and in the GASP polarimeter [70]. Some classes of cryogenic detectors have sub-microsecond time resolutions: Superconducting Tunnel Junctions (STJs) [184], Transition Edge Sensors (TES) [54] and Visible Light Photon Counters (VLPC) [154].

The high time cadence of modern surveys allows to identify a large number of transients and to send alerts for follow-up and the classification of transient type with spectroscopic observations. The foreseen frequency of alerts with the Large Synoptic Telescope is of the order of 10 millions per night, demanding a redefinition on the follow-up strategies.

---

<sup>52</sup><https://eventhorizontelescope.org/>

<sup>53</sup><https://www.skatelescope.org/>

## 10. Case Studies

Before the label multi-messenger achieved popularity, an astronomical event was observed over the electromagnetic spectrum and with neutrinos. Supernova SN 1987A was discovered on 1978 February 24.23 as a 5 magnitude object in the Large Magellanic Cloud [171], at a distance of about 50 kpc. A review of the event has been presented by [146]. SN 1987A is the first astrophysical source that produced particles detected on Earth. A neutrino burst was observed by the Kamiokande II instrument on February 23, 07:35:35 UT, during an interval of 13 seconds, with 11 events in the energy band from 7.5 to 36 MeV; the first two events pointed towards the direction the Large Magellanic Cloud within about 15 degrees [104]. The event was recorded by the IMB [100] and Baksan [45] detectors, with 8 and 5 neutrinos, respectively, within a few seconds. The neutrino detection occurred before the familiar brightening of the optical light curve.

### 10.1 GW150914

The detection of the GW150914 black hole merger provided the first direct detection of gravitational waves [5] (Fig. 23). Despite the electromagnetic emission is expected to be absent or weak, follow-up searches have been performed for GW150914 [6]. Fermi-GBM detected an unexpected weak transient above 50 keV, 0.4 s after the GW150914 event and lasting about 1 s, that was not observed by other instrument [71]. The transient was explained as a faint sGRB at a large angle [71]. Since there is no accretion material coming from tidal disruption, the binary black hole systems should have occurred in a site with existing material left from its previous history [140], [130], or be embedded in the disk of an active galactic nucleus [53]. The presence of material at the time of merger could lead to the production of jets [115], [150].

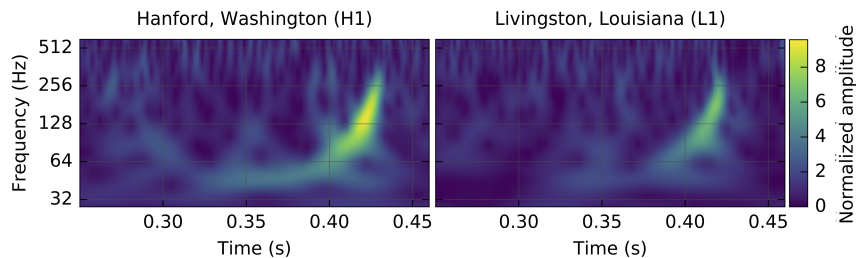


Figure 23: Spectrograms of the GW150914 signal in the LIGO-Hanford and LIGO-Livingston detectors; adapted from [5]

### 10.2 GW170817

The joint detection of the gravitational radiation from the binary neutron star merger GW170817 and from the short Gamma Ray Burst GRB 170817A is an example of multi-messenger astrophysics using gravitational waves and the whole electromagnetic spectrum [11], [13], [12].

On August 17, 2017 at 12:41:04 UTC the Advanced LIGO and Advanced Virgo instruments detected the event GW170817 [11] (Fig. 24, left). The gravitational source was localized within a sky region of  $28 \text{ deg}^2$  and at a luminosity distance of  $40_{-14}^{+8} \text{ Mpc}$  [11]. The gravitational signal was

associated to a binary neutron star merger [11], [18] and constrained the equation of state and the properties of neutron stars [16], [18], [19].

The Fermi-GBM and INTEGRAL SPI-ACS instruments detected the short Gamma Ray Burst GRB 170817A [95], [165], [13] with a delay of  $1.734 \pm 0.054$  s [13] with respect to the merger. The gravitational and gamma ray waveforms are shown in Fig. 24, right. The difference between the merger time and the gamma ray emission constrained the fractional difference between the speed of light and the speed of gravity in the interval between  $-3 \times 10^{-15}$  and  $+7 \times 10^{-16}$  c [13].

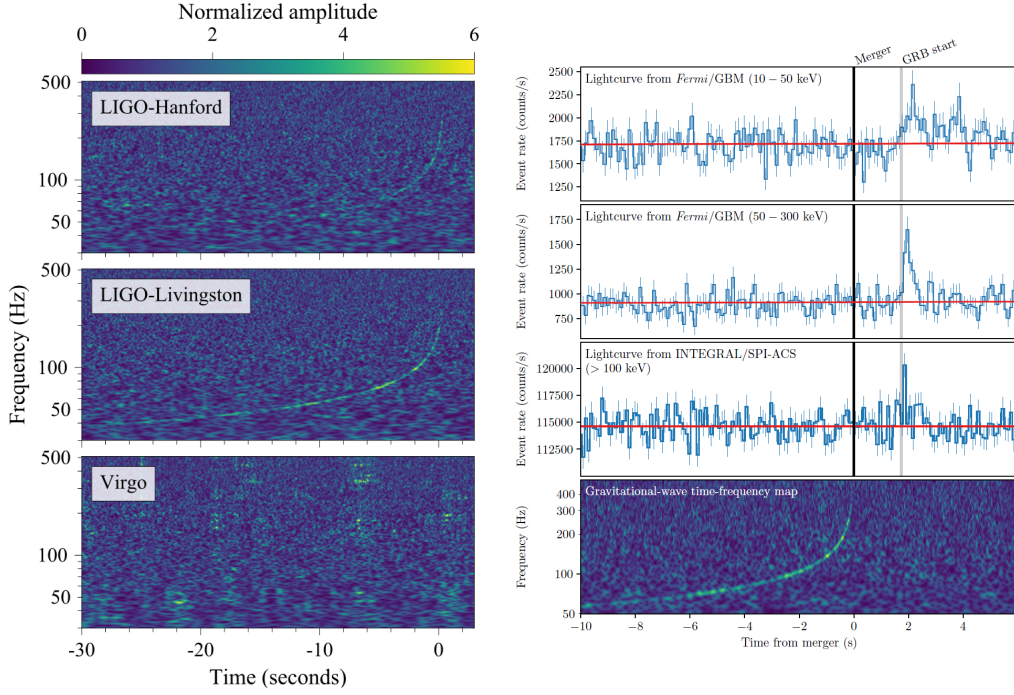


Figure 24: Left: spectrograms of the GW170817 signal in the LIGO-Hanford, LIGO-Livingston and Virgo detectors (adapted from [11]). Right: joint gravitational and electromagnetic detection of GW170817 and GRB 170817A. From top to bottom: Fermi-GBM light curve for GRB 170817A, 10-50 keV; the same as above, 50-300 keV; INTEGRAL SPI-ACS light curve above 100 keV; time-frequency map of GW170817 gravitational waveform (adapted from [13])

A worldwide observing campaign across the whole electromagnetic spectrum discovered an optical transient (SSS17a/AT 2017gfo) in the elliptical galaxy NGC 4993, located at a distance consistent with the gravitational luminosity distance. The first detection occurred 10.87 hours after the event by the One-Meter, Two-Hemisphere (1M2H) Collaboration with the 1m Swope telescope [73], [172] and was promptly confirmed by other observatories [183], [179], [129], [174], [48]. The source was not present in archival images secured a few weeks before the merger [183]. The transient AT 2017gfo was associated with the gravitational event GW170817 [12]. The light curves of GW170817/GRB 170817A/AT 2017gfo during the first weeks after the merger are shown in Fig. 25, left. The optical and infrared spectra showed the signatures of a kilonova, that evolved from a featureless blue continuum to the appearance of broad lanthanide features [170], [64], [135], [153], [132], [142], [117], [116], [120], [49], [74], [173], [82], [180], [126], [179], [69], in agreement

with the predictions of r-process nucleosynthesis in the ejecta and radioactive decay [127], [123], [136]. A selection of spectra is shown in Fig. 25, right.

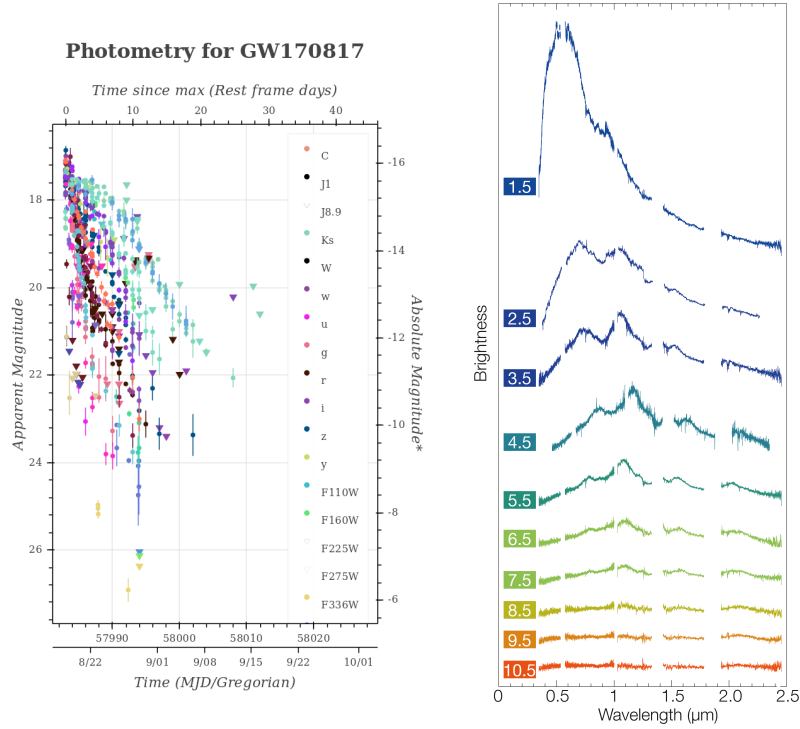


Figure 25: Left: light curve of GW170817 in different photometric bands in the first month after the merger (data from <https://kilonova.space/kne/GW170817/>); right: spectra of GW170817 in the first days after the merger (image credit: ESO/E. Pian et al./S. Smartt & ePESSTO)

The first X-ray and radio detections of the transient occurred at 9 and 16 days after the merger, respectively. The X-ray afterglow was discovered on 2017 Aug 26 with Chandra and showed a rising emission [180], [85], [99]. The radio afterglow was detected with the VLA on 2017 September 2 and showed a rising flux in the following weeks [101], [138]. The initial brightness rise observed in the X-rays, optical and radio observations [76], [132], [133], [181], [138], [121], [162] was followed by a turnover at about 149-170 days after the merger [162], [76], [133], [160], [139], [80], [44]. The afterglow evolution was consistent with an off-axis structured jet [180], [125] or a cocoon [138], [181], but not with a uniform jet.

No associated low energy or high energy neutrinos were observed in association to GW170817 neither within a  $\pm 500$  s window around the merger epoch nor in the 14 days after the merger. Upper limits have been set by The IceCube, ANTARES and Pierre Auger observatories (GeV-EeV and MeV energy ranges) [41], the Super-Kamiokande Observatory (3.5 MeV to 100 PeV) [22], the Baikal-GVD telescope (from TeV to 100 PeV) [50], the Baksan Underground Scintillation Telescope (above 1 GeV) [152].

The multi-messenger observations of GW170817 [11], [13], [12] show that the event was produced by the merger of two neutron stars, followed by the short gamma ray burst GRB 170817A and by a kilonova whose emission was powered by the radioactive decay of r-process nuclei syn-

thesized in the ejecta [84], [143], [144], [141], [59], [75], [52], [178]. Binary neutron star systems are the progenitors of short GRBs (or part of them).

The observation of GW170817 has allowed to probe the strong field dynamics of compact binaries and to test and set constraints on several aspects of General Relativity [13], [20]: difference between the speed of gravity and the speed of light, deviations from General Relativity in the Post Newtonian dynamics during the inspiral; anomalous dispersion of gravitational waves; violation of the Local Lorentz Invariance; number of large extra spatial dimensions; alternative polarization states. The detection of GW170817 has set limits on the stochastic background of gravitational waves [17].

The first observation of a gravitational event with an electromagnetic counterpart has produced an estimation of the Hubble constant completely independent on the electromagnetic determinations, since GW170817 is a standard siren, the gravitational equivalent of the standard candle [167]. The value of the Hubble constant measured with the value measured using CMB observations,  $67.8 \pm 0.9 \text{ km s}^{-1} \text{ Mpc}^{-1}$  [29], is in tension with the value estimated with Cepheids,  $73.48 \pm 1.66 \text{ km s}^{-1} \text{ Mpc}^{-1}$  [161]. The value of the Hubble constant estimated with the GW170817 event,  $70_{-8}^{+12} \text{ km s}^{-1} \text{ Mpc}^{-1}$ , has been determined by the combination of the gravitational distance with the recession velocity of the host galaxy NGC 4993 [14]. The precision on the Hubble constant achievable with additional GW170817 like events is 2% in five years and of 1% in ten years [68]. An alternative method to measure the Hubble constant is based on a statistical analysis of events without electromagnetic counterpart, considering the galaxies within the event localization region and combining the redshift of the contained galaxies with the gravitational estimated distance [88].

### 10.3 IceCube-170922A

The IceCube neutrino telescope detected a muon track from a neutrino interaction on 2017 September 22, triggering an alert within one minute and an extensive follow-up with a wide range of instruments [110]. The track pointed to the position of a known blazar, TXS 0506+056 [109], whose gamma ray emission increased around the same epoch [177], [137]. IceCube-170922A deposited an energy of  $23.7 \pm 2.8 \text{ TeV}$  in IceCube [110]. An analysis of data prior to the event showed a  $3\sigma$  neutrino excess in the direction of TXS 0506+056 before 2017 [111]. The ANTARES neutrino telescope did not find any neutrino candidate within  $\pm 1$  day around the event time [110], [42].

The follow-up of the IceCube-170922A event involved gamma rays, X-rays, optical and radio observatories. On September 28 the Fermi-LAT instrument reported that the direction of the neutrino was consistent with the position of the blazar TXS 0506+056, that at that epoch was showing an increased GeV emission [110]. The object had been previously observed by Fermi-LAT and had shown a brightening in the GeV band since 2017 April. The observations of the AGILE instrument in a 13 days window around the event were consistent with the Fermi-LAT observations [131]. The observations of TXS 0506+056 at very high energy with the Cherenkov instruments HESS, VERITAS, MAGIC showed no gamma ray emission during the first days [110], [23]. The source was detected on September 28 by MAGIC [110] up to 400 GeV. No source above 1 TeV was detected by the HAWC instrument [110]. The X-ray follow-up included Swift-XRT, NuSTAR, MAXI, INTEGRAL [110]. The observations with Swift showed an increased emission correlated with the increase of gamma ray emission [110]. The combination of gamma ray and X-ray obser-

uations showed a soft power spectrum in the Swift soft X-ray band, an hard power spectrum in the NuSTAR hard X-ray band and a power law spectrum with index 2 in the Fermi-LAT band. The redshift of TXS 0506+0506,  $0.3365 \pm 0.0010$ , was measured in an investigation triggered by the neutrino observation [145]. The gamma ray observations by Fermi-LAT and MAGIC are presented in Fig. 26.

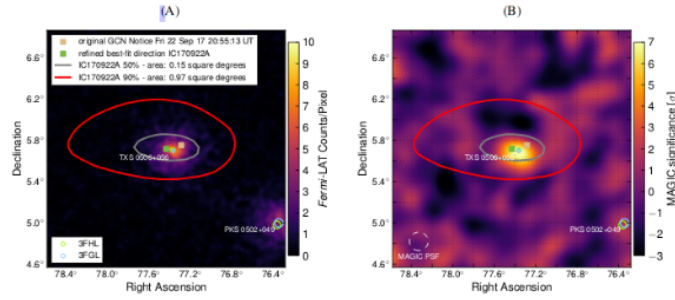


Figure 26: Fermi-LAT and MAGIC observations of TXS 0506+056; adapted from arXiv:1807.08816

The multi-messenger behavior of TXS 0506+056 in the months before the flare was reconstructed with the interplay of observations and archives (Fig. 27). The archival observations with ASAS-SN survey showed that TXS 0506+056 had achieved the highest flux in the recent years [110]. The blazar has been monitored by the Very Large Array in different bands from 2 to 20 GHz [110] after the neutrino event, showing a variable radio flux [110]. The observations with the OVRO telescope at 15 GHz show a progressive increase of the radio flux during the months before the neutrino event [110].

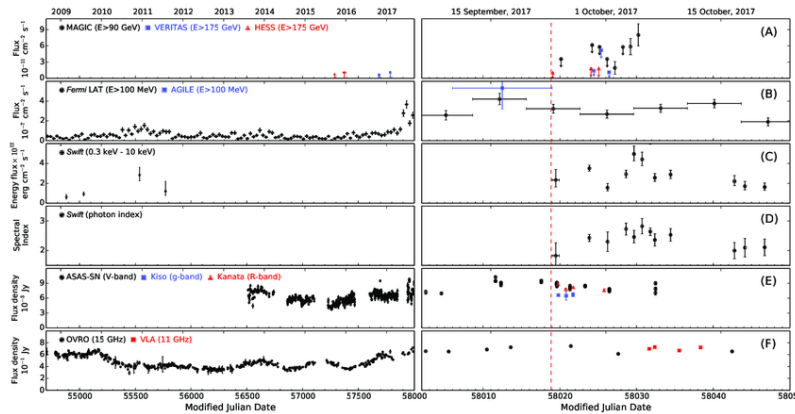


Figure 27: The multi-messenger light curves of TXS 0506+056; adapted from R. Reimann, Galaxies 7 (2019) 40

## 11. Preparing Future Multi-Messenger Astronomers

High energy astronomy encompasses experimental physics and observational astrophysics.

Physicists contribute to the building of the high energy instruments and use them as observational astronomers. The preparation of the next generation of multi-messenger astronomers requires the teaching of the techniques of the whole multi-messenger science, that involves a large number of astronomies, due to the different instruments and observational techniques involved. From the point of view of high energy astrophysics, optical and radio astronomy are related to the follow-up of high energy and gravitational events and to the search for possible progenitors. During the last years, the author has designed and taught courses on multi-messenger astronomy [155], [156], both as laboratory courses (Astrophysical Techniques) and as lecture course with in class sessions with open data (Experimental Methodologies for Astroparticle Physics). The lab experiments include: cosmic ray detection with plastic scintillators, gamma ray detection and spectroscopy (crystal scintillators with PMT and SiPMs); study of vibration modes with accelerometers (as in tests of Virgo/LIGO suspensions); optical observations at the telescope; measurement of the night sky brightness; CCD characterization; measurement of atmospheric transparency with photometers; radio astronomy instrumentation and sun transit observation at different radio frequencies with commercial receivers; solar flare detection at VLF frequencies. The data analysis sessions are based on open data of optical X-ray, gamma ray, gravitational observatories for a wide variety of sources (blazars, GRBs, pulsars, supernova remnants, gravitational events). Examples of multi-messenger investigation are the analysis of the time series of the GW150914 and GW170817 events, provided by LIGO LOSC<sup>54</sup>, accompanied by the study of the public electromagnetic observations of the second event.

## 12. Conclusions

The detection of gravitational waves and the observation of neutrinos from a blazar mark the beginning of multi-messenger astronomy, with electromagnetic spectrum, neutrinos, gravitational waves and cosmic rays providing complementary information about astrophysical sources. The combined use of all information carrier is accompanied by the exploration of astrophysical events over a broad interval of time scales. High energy astrophysical techniques are playing an increasing role in multi-messenger astronomy.

## References

- [1] A. Aab et al., *NIM A* **798** (2015) 172.
- [2] A. Aab et al., *Phys. Lett. B* **762** (2016) 288.
- [3] M. G. Aartsen et al., *PRL* **111** (2013) 021103.
- [4] M. G. Aartsen et al., arXiv:1910.08488. L194.
- [5] B. P. Abbott et al., *PRL* **116** (2016) 061102.
- [6] B. P. Abbott et al., *ApJ* **826** (2016) 13.
- [7] B. P. Abbott et al., *PRL* **116** (2016) 241103.
- [8] B. P. Abbott et al., *PRL* **118** (2017) 221101.
- [9] B. P. Abbott et al., *ApJ* **851** (2017) L35.

---

<sup>54</sup><https://www.gw-openscience.org/about/>

- [10] B. P. Abbott et al., *PRL* **119** (2017) 141101.
- [11] B. P. Abbott et al., *PRL* **119** (2017) 161101.
- [12] B. P. Abbott et al., *ApJL* **848** (2017) L12.
- [13] B. P. Abbott et al., *ApJL* **848** (2017) L13.
- [14] B. P. Abbott et al., *Nat* **551** (2017) 85.
- [15] B. P. Abbott et al., *CQG* **34** (2017) 044001.
- [16] B. P. Abbott et al., *PRL* **121** (2018) 161101.
- [17] B. P. Abbott et al., *PRL* **120** (2018) 091101.
- [18] B. P. Abbott et al., *PRX* **9** (2019) 011001.
- [19] B. P. Abbott et al., *PRL* **122** (2019) 061104.
- [20] B. P. Abbott et al., *PRL* **123** (2019) 011102.
- [21] B. P. Abbott et al., *PRX* **9** (2019) 031040.
- [22] K. Abe et al., *ApJ* **857** (2018) L4.
- [23] A. U. Abeysekara et al., *ApJ* **861** (2018) L20.
- [24] A. Achterberg et al., *AP* **26** (2006) 155.
- [25] M. Ackermann et al., *ApJ* **799** (2015) 86.
- [26] M. Ackermann et al., *PRL* **115** (2015) 231301.
- [27] M. Ackermann et al., *PRL* **116** (2016) 151105.
- [28] M. Ackermann et al., *ApJ* **840** (2017) 43.
- [29] P. A. R. Ade et al., *A&A* **594** (2016) A13.
- [30] S. Adrian-Martinez et al., *J. Phys. G* **43** (2016) 084001.
- [31] O. Adriani et al., *PRL* **105** (2010) 121101.
- [32] O. Adriani et al., *PRL* **111** (2013) 081102.
- [33] M. Aguilar et al., *PRL* **113** (2014) 121101.
- [34] M. Aguilar et al., *PRL* **113** (2014) 121102.
- [35] M. Aguilar et al., *PRL* **117** (2016) 091103.
- [36] M. Ageron et al., *NIM A* **656** (2011) 11.
- [37] F. Aharonian et al., *ApJ* **664** (2007) L71.
- [38] F. Aharonian et al., *A&A* **503** (2009) 817.
- [39] F. A. Aharonian, et al., *ApJ* **837** (2017) L15.
- [40] M. Ahlers and F. Halzen, *PPNP* **102** (2018) 73.
- [41] A. Albert et al., *ApJ* **850** (2017) L35.
- [42] A. Albert et al., *ApJ* **863** (2018) L30.
- [43] C. Alcock et al., *ApJL* **550** (2001) L169.

- [44] K. D. Alexander et al., *ApJ* **863** (2018) L18.
- [45] E. N. Alexeyev et al., *PLB* **205** (1988) 209.
- [46] P. Amaro-Seoane et al., arXiv:1702.00786.
- [47] E. Aprile et al., *PRL* **122** (2019) 141301.
- [48] I. Arcavi et al., *Nat* **551** (2017) 64.
- [49] I. Arcavi et al., *ApJL* **848** (2017) L33.
- [50] A. D. Avrorin et al., *JETPL* **108** (2018) 787.
- [51] C. Barbieri et al., *ASSP* **1570-6591** (2007) 249.
- [52] J. Barnes and D. Kasen, *ApJ* **775** (2013) 18.
- [53] I. Bartos et al., *ApJ* **835** (2017) 165.
- [54] T. L. Bay et al., *NIM A* **559** (2006) 506.
- [55] R. Bellazzini et al., *X-ray Polarimetry: A New Window in Astrophysics*, Cambridge University Press (2010)
- [56] E. C. Bellm et al., *PASP* **131** (2019) 018002.
- [57] I. A. Belolaptikov et al., *AP* **7** (1997) 263.
- [58] E. Berger et al., *ApJL* **774** (2013) L13.
- [59] E. Berger, *ARA&A* **52** (2014) 43.
- [60] R. Bernabei et al., *Phys. Part. Nucl.* **46** (2015) 138.
- [61] S. Bird et al., *PRL* **116** (2016) 201301.
- [62] T. D. Brandt, *ApJL* **824** (2016) L31.
- [63] A. G. A. Brown et al., *A&A* **616** (2018) A1.
- [64] D. A. H. Buckley et al., *MNRAS* **474** (2018) L71.
- [65] E. Bulbul et al., *ApJ* **789** (2014) 13.
- [66] B. Carr et al., *PRD* **96** (2017) 023514.
- [67] B. J. Carr and S. W. Hawking, *MNRAS* **168** (1974) 399.
- [68] H.-Y. Chen et al., *Nat* **562** (2018) 545.
- [69] R. Chornock et al., *ApJ* **848** (2017) L19.
- [70] P. P. Collins et al., PoS(CRAB2008)029.
- [71] V. Connaughton et al., *ApJ* **826** (2016) 6.
- [72] A. Cooray et al., *RSOS* **3** (2016) 150555.
- [73] D. A. Coulter et al., *Sci* **358** (2017) 1556.
- [74] P. S. Cowperthwaite et al., *ApJ* **848** (2017) L17.
- [75] P. D'Avanzo, *JHEAp* **7** (2015) 73.
- [76] P. D'Avanzo et al., *A&A* **613** (2018) L1.

- [77] R. Davis, *PP&NP* **32** (1994) 13.
- [78] A. De Angelis et al., *MNRAS* **432** (2013) 3245.
- [79] V. Dhillon et al., *MNRAS* **378** (2007) 825.
- [80] D. Dobie et al., *ApJ* **858** (2018) L15.
- [81] D. Dravins, *Mess.* **78** (1994) 9.
- [82] M. R. Drout et al., *Sci* **358** (2017) 1570.
- [83] N. Du et al., *PRL* **120** (2018) 151301.
- [84] D. Eichler et al., *Nat* **340** (1989) 126.
- [85] P. A. Evans et al., *Sci* **358** (2017) 1565.
- [86] The Event Horizon Telescope Collaboration, *ApJL* **875** (2019) L1.
- [87] F. Fenu et al., in Proceedings of *35th International Cosmic Ray Conference - ICRC2017*, [PoS \(ICRC2017\) 486](#) (2017).
- [88] M. Fishbach et al., *ApJ* **871** (2019) L13.
- [89] D. Gaggero et al., *PRL* **118** (2017) 241101.
- [90] Gaia Collaboration, *A&A* **595** (2016) A1.
- [91] J. P. Gardner et al., *SSR* **123** (2006) 485.
- [92] R. Gilmozzi and J. Spyromilio, *Msngr* **127** (2007) 11.
- [93] F. Giovannelli and L. Sabau-Graziati, *RMxAC* **45** (2014) 47.
- [94] F. Giovannelli, in Proceedings of *XII Multifrequency Behaviour of High Energy Cosmic Sources Workshop*, [PoS \(MULTIF2017\) 001](#) (2017).
- [95] A. Goldstein et al., *ApJ* **848** (2017) L14.
- [96] D. Gora et al., *Univ.* **4** (2018) 128.
- [97] K. Greisen, *PRL* **16** (1966) 748.
- [98] J. Grindlay et al., in *New Horizons in Time Domain Astronomy*, Proceedings IAU Symposium No. 285 (2011) 29.
- [99] D. Haggard et al., *ApJL* **848** (2017) L25.
- [100] T. Haines et al., *NIM A* **264** (1988) 28.
- [101] G. Hallinan et al., *Sci* **358** (2017) 1579.
- [102] F. Halzen, *NatPhys* **13** (2017) 232.
- [103] D. Harari et al., *JCAP* **11** (2006) 012.
- [104] K. Hirata et al., *PRL* **58** (1987) 1490.
- [105] E. M. Holt et al., in Proceedings of *35th International Cosmic Ray Conference - ICRC2017*, [PoS \(ICRC2017\) 492](#) (2017).
- [106] D. Hooper and L. Goodenough, *PL B* **697** (2011) 412.
- [107] R. Hudec, *AN* **339** (2018) 408.

- [108] IceCube Collaboration, *Sci* **342** (2013) 947.
- [109] IceCube Collaboration, *GCN* **21916** (2017).
- [110] The IceCube Collaboration et al., *Sci* **361** (2018) 146.
- [111] The IceCube Collaboration, *Sci* **361** (2018) 147.
- [112] Jun Luo et al., *CQG* **33** (2016) 035010.
- [113] G. Jungman et al., *Phys. Rep.* **267** (1996) 195.
- [114] G. Kanbach et al, *Proc. SPIE* **4841** (2003) 82.
- [115] A. Khan et al., *PRD* **97** (2018) 044036.
- [116] D. Kasen et al., *Nat* **551** (2017) 80.
- [117] M. M. Kasliwal et al., *Sci* **358** (2017) 6370.
- [118] U. F. Katz and Ch. Spiering, *PNPP* **67** (2012) 651.
- [119] H. Kawai et al., *Nucl. Phys. B Proc. Suppl.* **175** (2008) 221.
- [120] C. D. Kilpatrick et al., *Sci* **358** (2017) 1583.
- [121] S. Kim et al., *ApJ* **850** (2017) 850.
- [122] S. M. Koushiappas and A. Loeb, *PRL* **119** (2017) 041102.
- [123] S. Kulkarni, arXiv: astro-ph/0510256 (2005).
- [124] A. Kusenko, *Phys. Rep.* **481** (2009) 1.
- [125] D. Lazzati et al., *PRL* **120** (2018) 241103.
- [126] A. J. Levan et al., *ApJL* **848** (2017) L28.
- [127] L.-Z. Li and B. Paczynski, *ApJ* **507** (1998) 59.
- [128] V. Lipunov et al., *AdAst* **2010** (2010) 349171.
- [129] V. M. Lipunov et al., *ApJL* **850** (2017) L18.
- [130] A. Loeb, *ApJL* **819** (2016) L21.
- [131] F. Lucarelli et al., *ApJ* **870** (2019) 136.
- [132] J. D. Lyman et al., *NatAs* **2** (2018) 751.
- [133] R. Margutti et al., *ApJ* **856** (2018) L18.
- [134] T. A. Mathews and A. R. Sandage, *ApJ* **138** (1963) 30.
- [135] C. McCully et al., *ApJL* **848** (2017) L32.
- [136] B. D. Metzger, *LRR* **20** (2017) 3.
- [137] R. Mirzoyan, *ATel* **10817** (2017)
- [138] K. P. Mooley et al., *Nat* **554** (2018) 207.
- [139] K. P. Mooley et al., *ApJ* **868** (2018) L11.
- [140] K. Murase et al., *ApJL* **822** (2016) L9.
- [141] E. Nakar, *PhR* **442** (2007) 166.

- [142] M. Nicholl et al., *ApJ* **848** (2017) L18.
- [143] B. Paczynski, *ApJ* **304** (1986) 1.
- [144] B. Paczynski, *AcA* **41** (1991) 257.
- [145] S. Paiano et al., *ApJ* **854** (2018) 32.
- [146] N. Panagia, *CJA&AS* **8** (2008) 155.
- [147] <http://pdg.lbl.org>
- [148] R. D. Peccei and H. R. Quinn, *PRL* **38** (1977) 1440.
- [149] R. D. Peccei and H. R. Quinn, *PRD* **16** (1977) 1791.
- [150] R. Perna et al., *ApJ* **875** (2019) 49.
- [151] S. Petrera et al., *EPJ Web Conf.* **208** (2019) 08001.
- [152] V. B. Petkov et al., *JETP Lett.* **107** (2018) 398.
- [153] E. Pian et al., *Nat* **551** (2017) 67.
- [154] R. Poggiani, *ExA* **18** (2004) 109.
- [155] R. Poggiani, *Optical, Infrared and Radio Astronomy - From Techniques to Observation*, Springer (2017)
- [156] R. Poggiani, *High Energy Astrophysical Techniques*, Springer (2017)
- [157] G. Pojmanski, *AcA* **47** (1997) 467.
- [158] M. Punturo et al., *CQG* **27** (2010) 194002.
- [159] R. Racine, *ApJ* **159** (1970) L99.
- [160] L. Resmi et al., *ApJ* **867** (2018) 57.
- [161] A. G. Riess et al., *ApJ* **855** (2018) 136.
- [162] J. R. Ruan et al., *ApJ* **853** (2018) L4.
- [163] V. C. Rubin et al., *AJ* **67** (1962) 491.
- [164] M. Sasaki et al., *PRL* **117** (2016) 061101.
- [165] V. Savchenko et al., *ApJ* **848** (2017) L15.
- [166] M. Schumann, *J. Phys. G* **46** (2019) 103003.
- [167] B. F. Schutz, *Nat* **323** (1986) 310.
- [168] A. Sesana, *PRL* **116** (2016) 231102.
- [169] B. Shapiro et al., *Cryog.* **81** (2017) 83.
- [170] B. J. Shappee et al., *Sci* **358** (2017) 1574.
- [171] I. Shelton, *IAUC* **4316** (1987) 1.
- [172] M. R. Siebert et al., *ApJL* **848** (2017) L26.
- [173] S. J. Smartt et al., *Nat* **551** (2017) 75.
- [174] M. Soares-Santos et al., *ApJL* **848** (2017) L16.

- [175] C. Spiering, *EJP* **H37** (2012) 515.
- [176] A. W. Strong et al., *ARN&PS* **57** (2007) 285.
- [177] Y. T. Tanaka et al., *ATel* **791** (2017).
- [178] N. R. Tanvir et al., *Nat* **500** (2013) 547.
- [179] N. R. Tanvir et al., *ApJL* **848** (2017) L27.
- [180] E. Troja et al., *Nat* **551** (2017) 71.
- [181] E. Troja et al., *MNRAS* **478** (2018) L18.
- [182] O. Urban et al., *MNRAS* **451** (2015) 2447.
- [183] S. Valenti et al., *ApJL* **848** (2017) L24.
- [184] P. Verhoeve et al., *NIM A* **559** (2006) 598.
- [185] S. J. Wagner and A. Witzel, *ARA&A* **33** (1996) 163.
- [186] G. Z. Xie et al., *A&A* **220** (1989) 89.
- [187] D. G. York et al., Time Domain Research in Astronomy, White Paper for the 2009-2010 Decadal Survey Committee (2009).
- [188] G. T. Zatsepin and V. A. Kuzmin, *JETP Lett.* **4** (1966) 78.